IEEE Access
Multidisciplinary : Rapid Review : Open Access Journal

Design and Implementation of Quad-Element Super-Wideband MIMO Antenna for IoT Applications

Pawan Kumar[1], Shabana Urooj[2], and Areej Malibari[3]

[1]Department of Electrical Engineering, School of Engineering, Gautam Buddha University, Greater Noida 201312, India
[1]Virtuous Transactional Analytics Pvt. Ltd., Noida 201309, India
[2]Department of Electrical Engineering, College of Engineering, Princess Nourah Bint Abdulrahman University, Riyadh 84428, Saudi Arabia
[2]*(On leave)* Department of Electrical Engineering, School of Engineering, Gautam Buddha University, Greater Noida 201312, India
[3]Department of Computer Science, Faculty of Computing and IT, King Abdulaziz University, Jeddah 80200, Saudi Arabia
[3]College of Engineering, Princess Nourah Bint Abdulrahman University, Riyadh 84428, Saudi Arabia

Corresponding author: Shabana Urooj (SMUrooj@pnu.edu.sa).

ABSTRACT In this paper, a low-profile, compact, quad-port super-wideband (SWB) multiple-input–multiple-output (MIMO) antenna is presented for the internet of things (IoT) applications. The proposed antenna comprises four identical sickle-shaped resonating elements, which are excited by tapered coplanar waveguide (CPW) feed lines. The antenna elements are arranged in rotational symmetry (mutually orthogonal to each other) to achieve high port isolation. A complementary slot, which matches the sickle-shaped radiator, is etched from the ground of the proposed monopole antenna element to achieve massive bandwidth. The MIMO antenna possesses a resonating bandwidth ($|S_{11}| \leq -10$ dB) of 1.3–40 GHz and a bandwidth ratio of 31:1. In addition, an L-shaped slit and a complementary split-ring resonator (CSRR) are introduced in the sickle-shaped radiator to reject Bluetooth (2.4 GHz), WLAN (5.5 GHz), and downlink of X-band satellite communication (7.5 GHz) signals from the SWB. The proposed MIMO antenna is fabricated and experimental results are found in agreement with the simulated results.

INDEX TERMS IoT, isolation, MIMO, monopole, spatial diversity, SWB

I. INTRODUCTION

The internet of things (IoT) is a widely used term across the globe. In the coming years, billions of mobile devices and base station terminals will be connected through the internet to provide multiple IoT-based services. It is expected that by the end of the year 2020 more than 10 billion devices will be linked through IoT, while this number increases to 40 billion shortly. The IoT technology is used for converging various heterogeneous devices like wireless sensor networks, smart grids, control and automation systems, smart devices, etc. [1–2]. The selection of the antenna system being used in the IoT connected end-devices plays an important role in their functioning. Numerous factors, such as less design cost, low power consumption, simple hardware configuration, omnidirectional radiation patterns, need to be considered for designing an efficient antenna for IoT devices.

Moreover, the increasing demand for compact and portable devices miniaturizes the sizes of IoT modules. However, this poses a design challenge and compact-sized antennas are needed that can fit within the small available space while maintaining a reasonable performance under adverse fading/interference conditions [3–5].

In complex IoT modules, a low-profile, compact-sized, super-wideband (SWB) antenna could be the best option as it covers multiple wireless standards and technologies, which reduces the overall module size/weight [6–7]. Recently, several antenna designs have been investigated for the SWB [8–13]. A coplanar waveguide (CPW)-fed fractal antenna with dual iterations of the Sierpinski square slots was presented in [8]. The antenna showed a bandwidth ratio of 11:1. In [9], a microstrip line-fed modified star triangular fractal-shaped antenna with the semi-ellipse ground was reported. A CPW-fed octagonal-shaped antenna

with the defected ground surface (DGS) and four fractal iterations was investigated [10]. In [11], a fractal antenna with a hexagonal-shaped radiating element and a triangular slot was presented. In [12], a coaxial-fed antenna was modified by the second iteration of the octagonal fractal. An egg-shaped design was reported in [13], where the ground plane of the antenna was etched with a complementary slot. A comparatively larger area is required to design the SWB antenna with iterative combinations of the fractal geometries. Therefore, the employment of such designs in the multi-antenna configuration increases the overall dimensions of the antenna. Also, the designing and manufacturing of fractal antennas is a difficult process. Several other SWB antenna designs with dual-branch feed, tapered feed, asymmetric coplanar strip (ACS), asymmetric ground plane, self-complementary, and curve boundaries were also reported [14–18]. In [14], an antenna consisted of two parallelly arranged loop patches, which were linked with the triangular sectors and symmetry axis, was reported. A dual-branch fed rectangular-shaped antenna with an asymmetric trapezoidal-shaped ground plane was proposed [15]. In [16], a compact ACS-fed antenna consisted of a boomerang-shaped strip and a hexagonal-shaped loop was reported. A microstrip balun-fed modified bowtie antenna was presented for microwaves and millimeter-waves [17]. In [18], an antenna consisted of an elliptical-shaped radiator and a trapezoidal ground surface was reported.

The next-generation mobile networks must support simultaneous operation of low data rate, such as low power sensors, and high data rate (for example, high-definition live video streaming) systems. A system with multiple-input–multiple-output (MIMO) array and super-wide bandwidth seem to be a promising candidate to fulfill the data rate requirements [19–20]. In [21], a two-port SWB MIMO antenna consisted of diagonally placed quarter-circular patches and orthogonally arranged ground surfaces was investigated. The antenna bandwidth ratio was 26:1. A two-port MIMO antenna consisted of tapered microstrip line-fed semi-circular shaped antenna elements was reported [22], where a corrugated T-shaped parasitic element was employed for better port isolation. An antenna consisted of two feather-shaped radiating elements was designed [23], where a metal strip was introduced between the antenna elements for isolation enhancement. A dual-port antenna consisted of elliptical-shaped radiators was reported [24], where WLAN and Wi-MAX bands were notched from the SWB by etching split-ring resonator (SRR) and spiral microstrip defected structure from the patch and the feeding, respectively. A MIMO antenna consisted of four spade-shaped radiators and a windmill-shaped decoupling element was presented [25], where an elliptical slot was etched on the antenna element to improve its radiation performance. A MIMO antenna consisted of four semi-elliptical resonating elements was reported in

[26], where triple notched bands were achieved by etching an L-shaped element and a complementary split-ring resonator (CSRR) on the patch. However, the SWB MIMO antenna configurations reported so far mainly comprised of two antenna elements [21–24] and one or two notched bands [24]. A few SWB antenna designs were presented with four resonating elements [25–26] and triple notched-band features [26], but their large sizes may limit their applications in compact IoT modules. Also, the ground of the antenna elements in [21], [23], [25] are not interconnected, therefore, these antennas might not be used for practical MIMO applications.

In this work, a compact-sized four-element MIMO antenna is designed for the SWB frequency range. Each resonator of the presented MIMO antenna consists of a tapered feedline, a sickle-shaped resonator, and a modified ground plane. A slot complementary to the sickle-shaped element is carved from the ground of the monopole antenna for achieving the SWB. Also, a CSRR and an L-shaped slit are implanted in the sickle-shaped patch to obtain triple notched bands. A CSRR is made up of two concentric circular rings of the same width and different radii, and it eliminates the WLAN and downlink of X-band satellite communication from the SWB. The resonating elements are located orthogonal to each other to obtain high isolation between them. The connected ground planes [27] of the antenna elements, and coplanar design [28], where the radiators and the ground are printed on the same surface of the dielectric substrate, offers simple integration of the MIMO antenna into IoT modules.

II. ANTENNA CONFIGURATION

A. SWB ANTENNA ELEMENT DESIGN

A schematic of the proposed SWB antenna element is shown in Fig. 1. The antenna element consists of a sickle-shaped resonating patch, a modified ground surface, and a tapered feed line that offers efficient matching in a wideband frequency range.
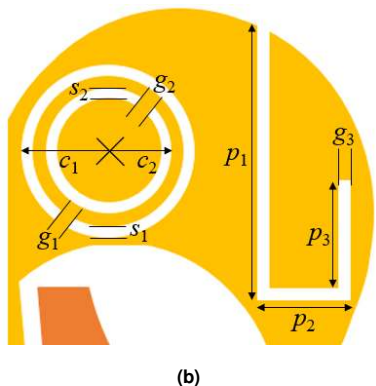

(a)

(b)
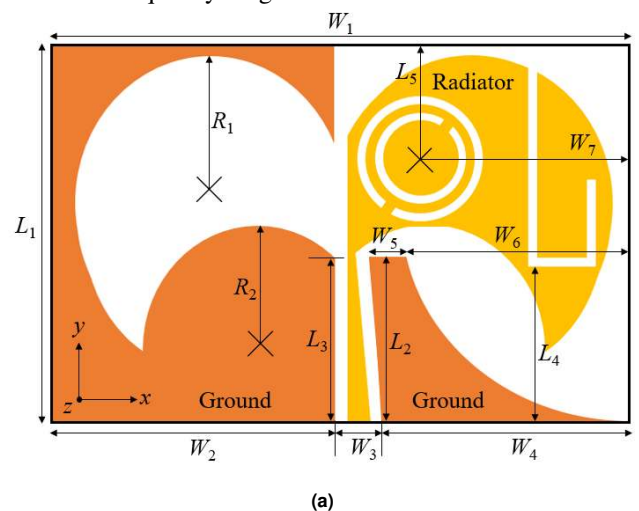
FIGURE 1. Sickle-shaped antenna element: (a) layout, (b) expanded view of the notched-band slits.

A complementary sickle-shaped slot is etched from the ground surface of the monopole antenna to obtain the SWB. A CSRR and an L-shaped slit are etched from the sickle-shaped patch to obtain triple notched bands at 2.4 GHz, 5.5 GHz, and 7.5 GHz. A CSRR and an L-shaped slit are etched from the sickle-shaped patch to obtain triple notched bands at 2.4 GHz, 5.5 GHz, and 7.5 GHz. Rogers RO4003C substrate material (of relative permittivity (ε_r) of 3.38, loss tangent (tan δ) of 0.0027, and thickness of 0.5 mm) is used for the fabrication of the prototype antenna. The dimensions of the triple notched-band sickle-shaped antenna element are displayed in Table I. The development and optimization of the antenna are performed using the simulation tool ANSYS HFSS®. The designed SWB antenna element size is 22×34 mm².

TABLE I
DESIGN DETAILS OF THE SICKLE-SHAPED ANTENNA ELEMENT AND MIMO ANTENNA

Dimensions	Value (mm)	Dimensions	Value (mm)
L_1	22	c_1	3.65
W_1	34	c_2	2.65
W_2	17	g_1	0.6
W_3	3	g_2	0.6
W_4	14	g_3	0.5
L_2	9.5	s_1	0.4
L_3	9.5	s_2	0.4
L_4	9.6	p_1	11.1
L_5	6.5	p_2	3.9
W_5	2	p_3	4.4
W_6	12.5	U_1	56
W_7	11.5	V_1	56
R_1	7	W_8	16.9
R_2	5.5	c_3	6

1) DESIGN PROCESS

In Fig. 2(a), a planar monopole antenna is chosen (step-1) as it shows wide bandwidth and simple geometry. The antenna element consists of a truncated heart-shaped radiator, a feed line, and a rectangular ground plane. The proposed monopole antenna displays wide operating bandwidth as demonstrated in Fig. 3(a). In step-2, the antenna element is modified to a sickle-shaped self-

complementary structure to achieve an ultra-wide frequency range. Mushiake's relationship demonstrates that the input impedance of a self-complementary antenna (SCA) is constant [29]

$$Z_{in} = \frac{z_0}{2} \approx 188.5 \ \Omega \qquad (1)$$

where Z_0 signifies the calculated impedance in free space. The given relationship demonstrates that the input impedance of a self-complementary design is not affected by the antenna wavelength, bandwidth, and dimensions. This approach is useful for designing antennas with large bandwidth [30–31]. As shown in Fig. 2(b), a slot analogous to the radiator is carved from the monopole antenna ground surface to achieve a broader bandwidth.
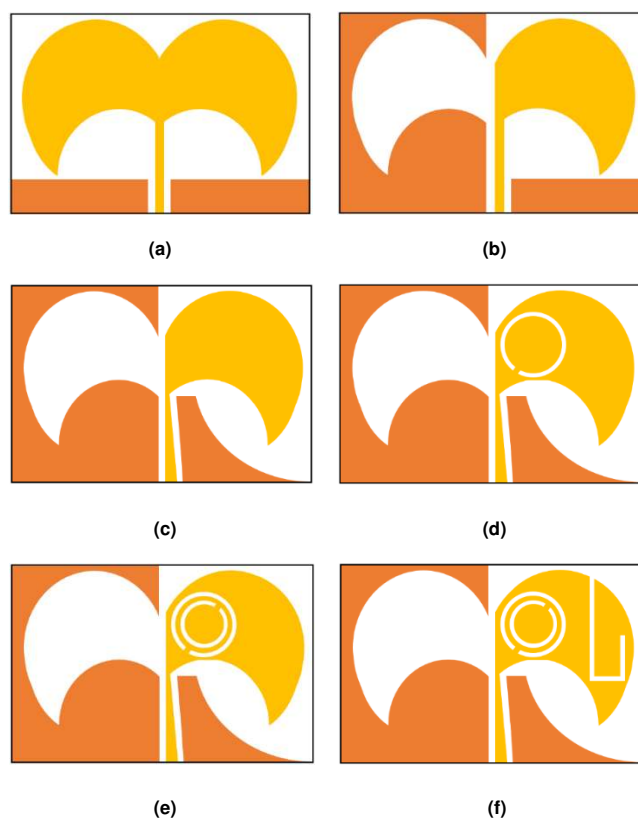

FIGURE 2. Evolution of the sickle-shaped antenna element: (a) step-1, (b) step-2, (c) step-3, (d) step-4, (e) step-5, (f) step-6.

In step-3, the smaller ground plane and feed line of the SCA is modified to the tapered triangular (shown in Fig. 2(c)) to improve the impedance matching and obtain the SWB frequency range. The S_{11} response of the SWB SCA element is displayed in Fig. 3(a). It is observed that the sickle-shaped antenna element exhibits a bandwidth of 1.3–40 GHz.

In step-4, an SRR is etched on the sickle-shaped antenna element as displayed in Fig. 2(d). The SRR removes the interrupting 5.5 GHz band (WLAN) from the SWB
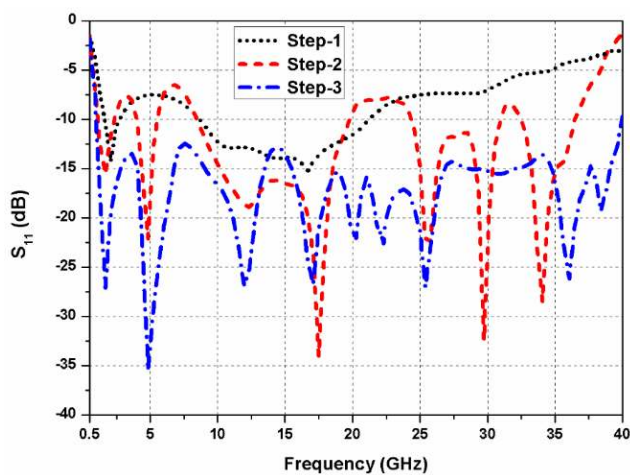
spectrum. The effective length of SRR (S_{Ro}) is calculated as [32]

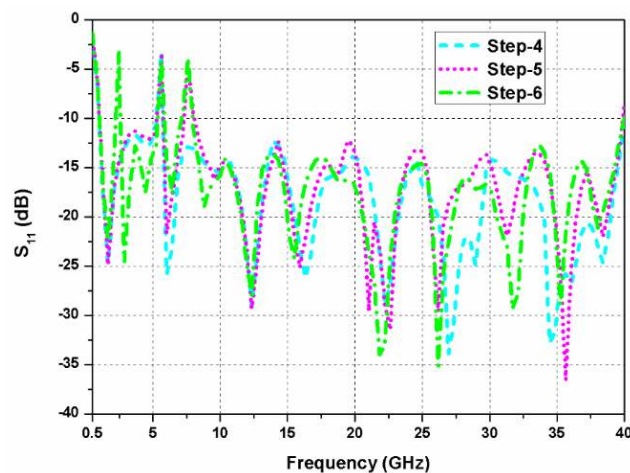$$S_{Ro} = \{\pi(2c_1 - s_1) - g_1\} \approx 0.5\lambda_{gi} \qquad (2)$$

$$\lambda_{gi} = \frac{c}{f_c}\left(\frac{1}{\sqrt{\varepsilon_{r,eff}}}\right), i = 1, 2, 3 \qquad (3)$$

$$\varepsilon_{r,eff} = \frac{\varepsilon_r + 1}{2} \qquad (4)$$

where λ_{gi} and f_c are guided wavelength and center frequency of the notched band, respectively, c is the velocity of light in free space, and $\varepsilon_{r,eff}$ is the effective relative permittivity of the dielectric substrate.

(a)

(b)

FIGURE 3. Simulated S_{11} response of the evolution steps: (a) step-1, -2, and -3, (b) step-4, -5, and -6.

In the next step (step-5), another SRR is etched on the sickle-shaped patch to eliminate the interfering 7.5 GHz band (downlink of X-band satellite communication) as

shown in Fig. 2(e). The effective length of inner SRR (S_{Ri}) is calculated as [32]

$$S_{Ri} = \{\pi(2c_2 - s_2) - g_2\} \approx 0.5\lambda_{gi} \qquad (5)$$

As shown in Fig. 2(f), in step-6, an L-shaped slit is engraved on the radiating patch (step-6) to remove 2.4 GHz (Bluetooth) interfering signals. The effective length of the L-shaped slit (S_L) is evaluated as [32]

$$S_L = (p_1 + p_2 + p_3 + g_3) \approx 0.25\lambda_{gi} \qquad (6)$$

The S_{11} response of the sickle-shaped antenna element design steps (-4, -5, and -6) is shown in Fig. 3(b).
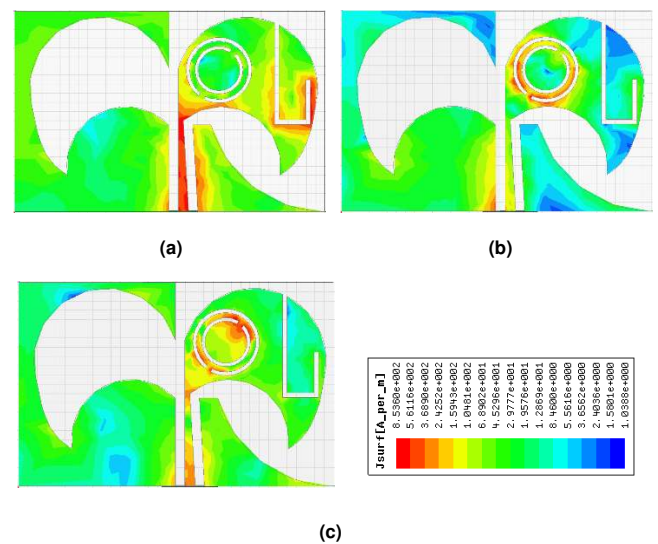

FIGURE 4. Simulated electric field in the sickle-shaped antenna element: (a) 2.4 GHz, (b) 5.5 GHz, (c) 7.5 GHz.

The current distribution of the sickle-shaped antenna element at frequencies 2.4 GHz, 5.5 GHz, and 7.5 GHz is shown in Fig. 4. It is observed from Fig. 4(a) that current is primarily present alongside the L-shaped slit, which is responsible for notching the Bluetooth frequency from the SWB. In Fig. 4(b), a stronger current magnitude is visible around the outer SRR, which rejects the WLAN band. Similarly, a strong current is found near to the inner SRR, as shown in Fig. 4(c), which is responsible for rejecting the X-band satellite communication signals. Hence, a triple notched-band performance is achieved by etching a CSRR and an L-shaped slit from the sickle-shaped antenna element.

B. SWB MIMO ANTENNA
The dimensions of the antenna element must be kept small for the smooth installation of the MIMO antenna in the IoT modules [7]. But, designing a small-sized four-port MIMO antenna is challenging due to the correlation between the neighboring antenna elements. In this work, a small-sized

four-port MIMO antenna is designed for the SWB spectrum range. Fig. 6 displays the layout of the proposed MIMO antenna. The resonator ground planes are attached to achieve the same reference voltage. Also, the four antenna elements are located in an orthogonal manner, and the diagonal radiators are arranged in anti-parallel orientation to decrease the inter-element coupling and achieve polarization diversity. The total size of the designed four-element SWB MIMO antenna is $56 \times 56 \times 0.5$ mm^3.
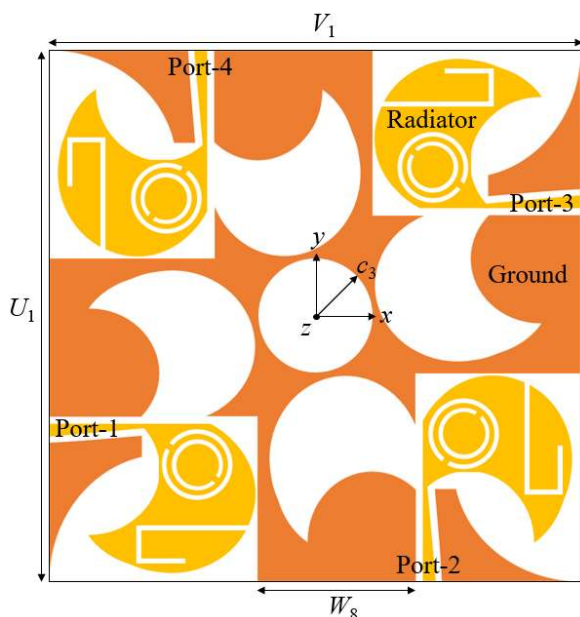

FIGURE 5. Layout of the four-element SWB MIMO antenna.

III. RESULTS DISCUSSION

The S_{11} response of the designed MIMO antenna is displayed in Fig. 6. The ($|S_{11}| \leq -10$ dB) bandwidth of the four-element MIMO antenna is 1.3–40 GHz with a bandwidth ratio of 31:1. The CSRR and L-shaped slit eliminates the Bluetooth (2.4 GHz), WLAN (5.5 GHz), and downlink of X-band satellite communication (7.5 GHz) signals from the SWB. The three notches can be varied by altering the dimensions of the CSRR and L-shaped slit.

When the measurements are carried at one antenna port, the other ports are terminated through the matching load of 50-Ω. The availability of the ordinary SMA connectors and limited resources limits the experimental results only up to 18 GHz. The mutual coupling between different sickle-shaped antenna elements is shown in Figs. 7(a) and (b). At lower frequencies, the inter-element isolation achieved is larger than 22 dB, and it increases toward higher frequency range.

The peak gain of the antenna is about 7 dBi as displayed in Fig. 8. Satisfactory gain values are seen in the antenna resonance band except for the three notched bands. A sharp dip in the gain curve at 2.4 GHz, 5.5 GHz, and 7.5 GHz validates that the antenna suppresses the Bluetooth, WLAN,

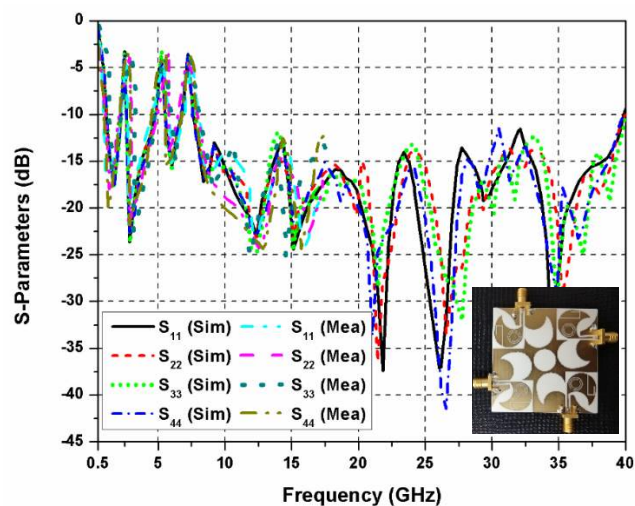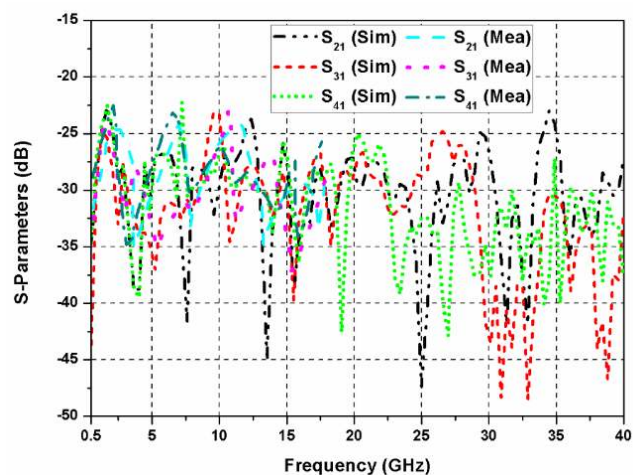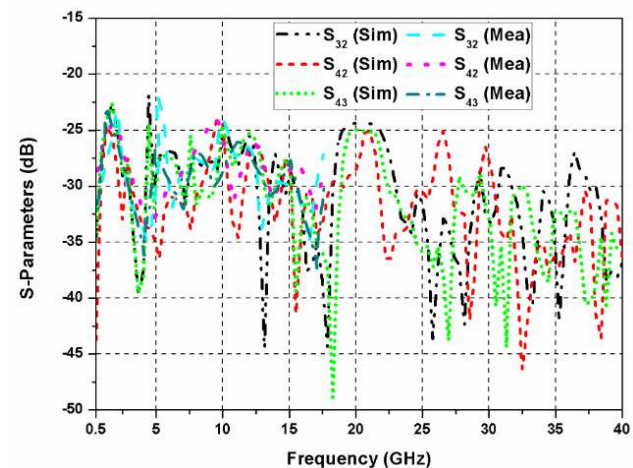and X-band satellite communication signals from the SWB.

FIGURE 6. Simulated and measured S_{11}, S_{22}, S_{33}, and S_{44} of the four-element SWB MIMO antenna.

(a)

(b)

FIGURE 7. Simulated and measured *S*-parameters of the four-element

IEEE *Access*

Multidisciplinary : Rapid Review : Open Access Journal

SWB MIMO antenna: (a) S_{21}, S_{31}, and S_{41}, (b) S_{32}, S_{42}, and S_{43}.
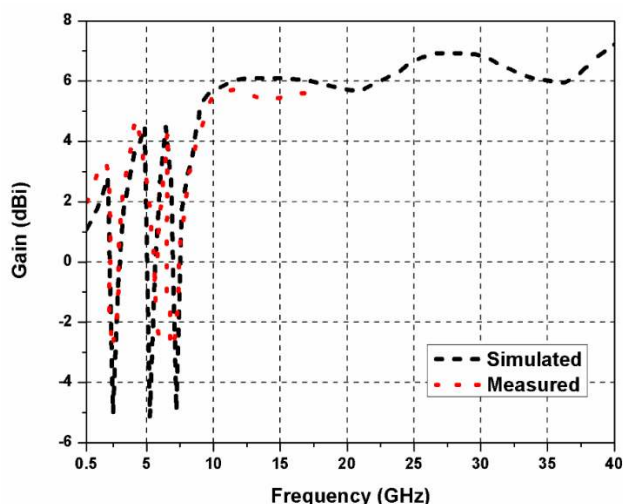

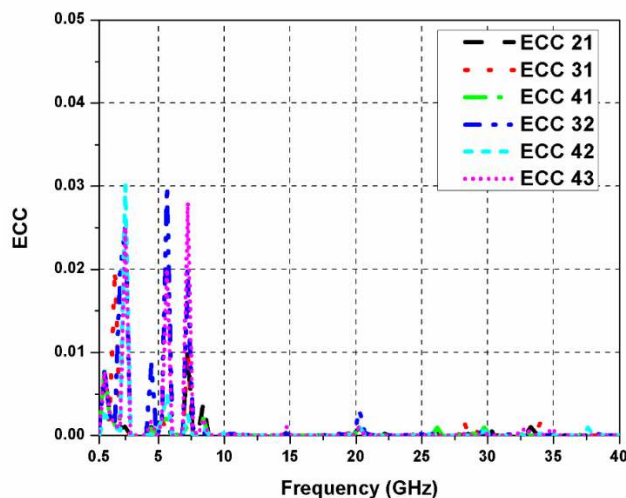**FIGURE 8.** Gain response of the four-element SWB MIMO antenna.

FIGURE 9. ECC curves of the four-element SWB MIMO antenna.

The diversity performance of the MIMO system can be predicted through the envelope correlation coefficient (ECC). The ECC value between the element-1 and element-2 of the MIMO antenna can be calculated as [33]

$$\rho_e = \frac{\left|\iint [\vec{F_1}(\theta,\varphi)\vec{F_2}(\theta,\varphi)]\, d\Omega\right|^2}{\iint |\vec{F_1}(\theta,\varphi)|^2\, d\Omega \iint |\vec{F_2}(\theta,\varphi)|^2\, d\Omega} \qquad (7)$$

where F is the radiated field, Ω, θ, and φ are the solid, elevation, and azimuthal angles, respectively. A similar procedure is used to compute ECC values between other antenna ports. For the proposed MIMO antenna, the ECC between different ports is less than 0.03 for the entire SWB frequency range.

The current distribution of the MIMO antenna is displayed in Fig. 10, where all the sickle-shaped antenna elements are excited simultaneously. In Fig. 10(a), it is noticed that the current concentrates around the L-shaped resonator at 2.4 GHz. Similarly, a strong current is seen around the outer and inner SRRs, shown in Figs. 8(b) and (c), which are accountable for eliminating the WLAN (5.5 GHz) and downlink satellite communication X-band (7.5 GHz) frequencies, respectively.
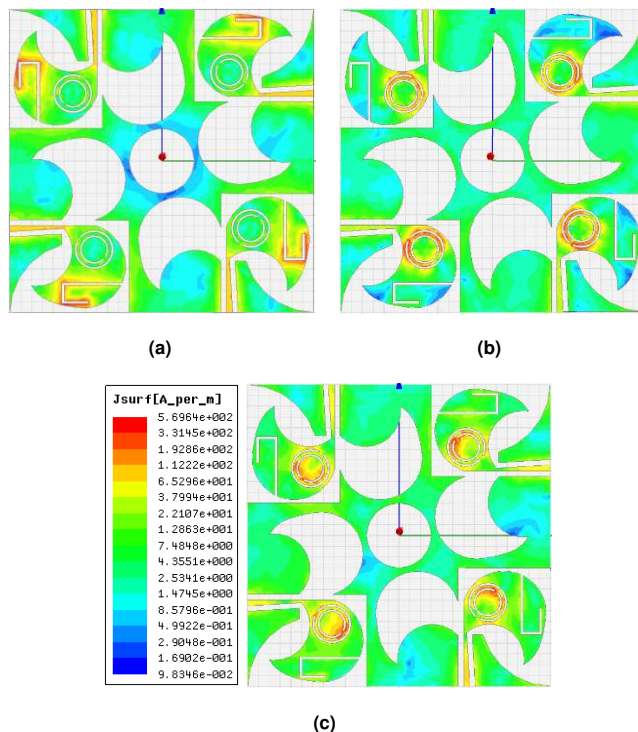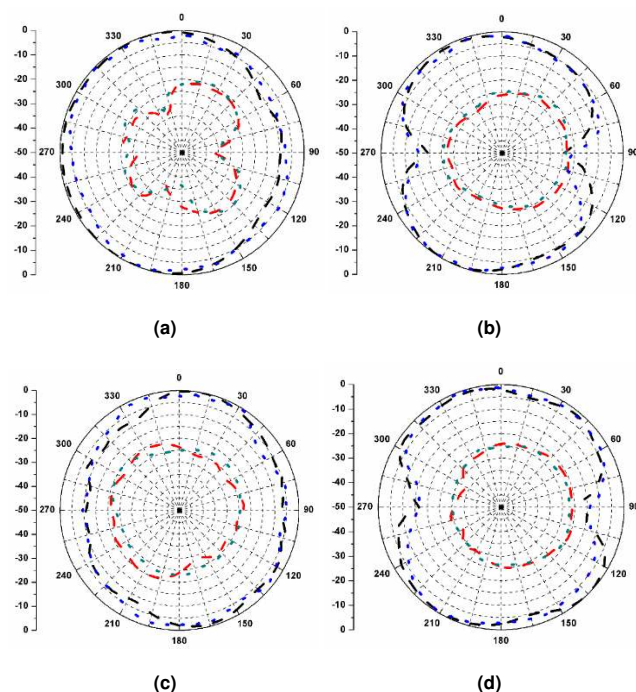

(a)

(b)

(c)

FIGURE 10. Simulated electric field in the MIMO antenna: (a) 2.4 GHz, (b) 5.5 GHz, (c) 7.5 GHz.
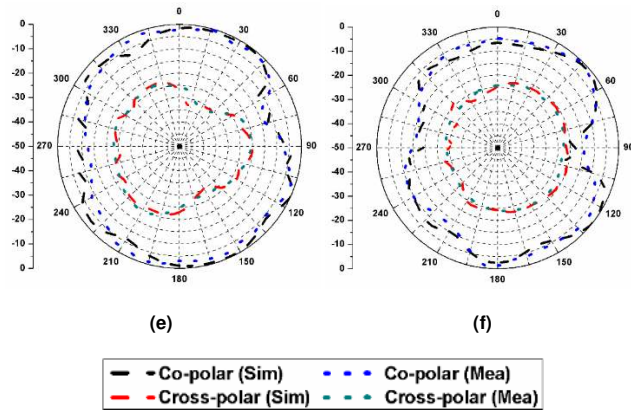

(a)

(b)

(c)

(d)

FIGURE 11. Measured and simulated patterns of the antenna: (a) H-plane, 6 GHz, (b) E-plane, 6 GHz, (c) H-plane, 11 GHz, (d) E-plane, 11 GHz, (e) H-plane, 16 GHz, (f E-plane, 16 GHz.

The measured and simulated patterns of the proposed SWB MIMO antenna at 6 GHz, 11 GHz, and 16 GHz are given in Fig. 11. The co-polar and cross-polar radiation patterns display a difference of more than 15 dB in both E-plane and H-plane, which shows the stable radiation characteristics of the designed antenna. The omni-directional pattern is observed in the H-plane and bi-directional patterns in the E-plane.

A comparison of the proposed antenna and previously designed SWB MIMO antennas is given in Table II. The proposed MIMO antenna has numerous benefits over the antennas reported previously [21–26], in terms of compact size, bandwidth ratio, notched bands, isolation between antenna ports, and the number of resonators. In the proposed

antenna, the signals (at 2.4 GHz, 5.5 GHz, and 7.5 GHz) are rejected without using any active devices or filtering circuitry. The use of filtering circuitry for the elimination of interfering frequency bands makes the antenna integration process difficult as it leads to a bulky design that requires more space. The polarization diversity and better isolation are achieved between the antenna elements by arranging them in orthogonal and anti-parallel orientation. The coplanar geometry of the proposed design is advantageous as it offers simple integration of the MIMO antenna into IoT modules. Stable performance is achieved due to the common or interconnected ground planes of the proposed MIMO antenna.

IV. CONCLUSION

A compact four-element SWB MIMO antenna is presented with triple notched-band feature. The proposed MIMO antenna contains four identical sickle-shaped resonating elements and a common ground plane. SWB properties are achieved by introducing a radiator matching slot (complementary) in the ground of the monopole antenna element. In the sickle-shaped antenna element, a CSRR and an L-shaped slit are etched to eliminate the Bluetooth, WLAN, and satellite communication X-band signals. The operating range of the MIMO antenna varies from 3.1 to 40 GHz, and an agreement is seen between the experimental and simulated data. The antenna performs well and shows omni-directional radiation patterns, high isolation, and low ECC. The coplanar profile and lightweight of the antenna allow its easy integration into the IoT modules/devices.

TABLE II
COMPARISON OF THE DESIGNED SWB MIMO ANTENNA WITH THE EXISTING DESIGNS

Ref.	Number of ports	Antenna size (mm^3)	Bandwidth ratio	Impedance bandwidth (GHz)	Number of notch bands	Notched band central frequency (GHz)	Isolation (dB)	ECC
[21]	2	$130 \times 120 \times 0.787$	26:1	1.04–27.2	---	---	>10	<–10 dB
[22]	2	$40 \times 47 \times 1.5$	31:1	1.3–40	---	---	>20	<0.02
[23]	2	$31 \times 31 \times 1.6$	14:1	3.8–51.5	---	---	>15	<–30 dB
[24]	2	20×36	28:1	1.21–34	2	3.5, 5.5	>15	<0.25
[25]	4	$58 \times 58 \times 1$	14:1	2.9–40	---	---	>17	<0.04
[26]	4	$63 \times 63 \times 1.6$	31:1	1.3–40	3	3.5, 5.5, 8.5	>16	<0.01
This work	4	$56 \times 56 \times 0.5$	31:1	1.3–40	3	2.4, 5.5, 7.5	>22	<0.03

REFERENCES

[1] Khanna, A.; Kaur, S. Internet of things (IoT), applications and challenges: A comprehensive review. *Wireless Pers. Commun.* **2020**, *114*, 1687–1762.

[2] Ejaz, W.; Anpalagan, A.; Imran, M.A.; Jo, M.; Naeem, M.; Qaisar, S.B.; Wang, W. Internet of things (IoT) in 5G wireless communications. *IEEE Access* **2016**, *4*, 10310–10314.

[3] Jha, K.R.; Bukhari, B.; Singh, C.; Mishra, G.; Sharma, S.K. Compact planar multistandard MIMO antenna for IoT applications. *IEEE Trans. Antennas Propag.* **2018**, *66*, 3327–3336.

[4] Lizzi, L.; Ferrero, F. Use of ultra-narrow band miniature antennas for internet-of-things applications. *Electron. Lett.* **2015**, *51*, 1964–1966.

[5] Awais, Q.; Chattha, H.T.; Jamil, M.; Jin, Y.; Tahir, F.A.; Rehman, M.U. A novel dual ultrawideband CPW-fed printed antenna for internet of things (IoT) applications. *Wirel. Commun. Mob. Comput.* **2018**, 2179571.

[6] An, W.; Zhang, P.; Xu, J.; Luo, H.; Huang, L.; Zhong, S. A novel machine learning aided antenna selection scheme for MIMO internet of things. *Sensors* **2020**, *20*, 2250.

[7] Johannsen, N.L.; Peitzmeier, N.; Hoeher, P.A.; Manteuffel, D. On the feasibility of multi-mode antennas in UWB and IoT applications below 10 GHz. *IEEE Commun. Mag.* **2020**, *58*, 69–75.

[8] Singhal, S.; Singh, A.K. CPW-fed hexagonal Sierpinski super wideband fractal antenna. *IET Microw. Antennas Propag.* **2016**, *10*, 1701–1707.

[9] Waladi, V.; Mohammadi, N.; Zehforoosh, Y.; Habashi, A.; Nourinia, J. A novel modified star-triangular fractal (MSTF) monopole antenna for super-wideband applications. *IEEE Antennas Wireless Propag. Lett.* **2013**, *12*, 651–654.

[10] Singhal, S.; Singh, A.K. CPW-fed octagonal super-wideband fractal antenna with defected ground structure. *IET Microw. Antennas Propag.* **2017**, *11*, 370–377.

[11] Shahu, B.L.; Pal, S.; Chattoraj, N. Design of super wideband hexagonal-shaped fractal antenna with triangular slot. *Microw Opt. Technol. Lett.* **2015**; *57*, 1659–1662.

[12] Azari, A. A new super wideband fractal microstrip antenna. *IEEE Trans. Antennas Propag.* **2011**, *59*, 1724–1727.

[13] Chen, K.; Sim, C.; Row, J. A compact monopole antenna for super wideband applications. *IEEE Antennas Wireless Propag. Lett.* **2011**, *10*, 488–491.

[14] Yeo, J.; Lee, J. Coupled-sectorial-loop antenna with circular sectors for super wideband applications. *Microw Opt. Technol. Lett.* **2014**, *56*, 1683–1689.

[15] Liu, J.; Esselle, K.P.; Hay, S.G.; Zhong, S.S. Compact super-wideband asymmetric monopole antenna with dual-branch feed for bandwidth enhancement. *Electron. Lett.* **2013**, *49*, 515–516.

[16] Trinh-Van, S.; Kwon, G.; Hwang, K.C. Planar super-wideband loop antenna with asymmetric coplanar strip feed. *Electron. Lett.* **2016**, *52*, 96–98.

[17] Yurduseven, O.; Smith, D.; Elsdon, M. Printed slot loaded bow-tie antenna with super wideband radiation characteristics for imaging applications. *IEEE Trans. Antennas Propag.* **2013**, *61*, 6206–6210.

[18] Zhong, S.; Liang, X.; Wang, W. Compact elliptical monopole antenna with impedance bandwidth in excess of 21:1. *IEEE Trans. Antennas Propag.* **2007**, *55*, 3082–3085.

[19] Obara, T.; Okuyama, T.; Inoue, Y.; Aoki, Y.; Suyama, S.; Lee, J.; Okumura, Y. Experimental trial of 5G super wideband wireless systems using massive MIMO beamforming and beam tracking control in 28GHz band, *IEICE Trans. Commun.* **2017**, *E100.B*, 1256–1268.

[20] Aziz ul Haq, M.; Koziel, S. Feedline alterations for optimization-based design of compact super-wideband MIMO antennas in parallel configuration. *IEEE Antennas Wireless Propag. Lett.* **2019**, *18*, 1986–1990.

[21] Liu, J.; Esselle, K.P.; Hay, S.G.; Sun, Z.; Zhong, S. A compact super-wideband antenna pair with polarization diversity. *IEEE Antennas Wireless Propag. Lett.* **2013**, *12*, 1472–1475.

[22] Ullah, H.; Rahman, S.U.; Cao, Q.; Khan, I.; Ullah, H. Design of SWB MIMO antenna with extremely wideband isolation. *Electronics* **2020**, *9*, 194.

[23] Singhal, S. Feather-shaped super wideband MIMO antenna. *Int. J. Microw. Wireless Technol.* **2020**, 1–9. (doi:10.1017/S1759078720000549)

[24] Bhattacharya, A.; Roy, B.; Bhattacharjee, A.K. Compact, isolation enhanced, band-notched SWB–MIMO antenna suited for wireless personal communications. *Wireless Pers. Commun.* **2020**. (doi: 10.1007/s11277-020-07749-6)

[25] Yu, C.; Yang, S.; Chen, Y.; Wang, W.; Zhang, L.; Li, B.; Wang, L. A super-wideband and high isolation MIMO antenna system using a windmill-shaped decoupling structure. *IEEE Access* **2020**, *8*, 115767–115777.

[26] Kumar, P.; Urooj, S.; Alrowais, F. Design of quad-port MIMO/diversity antenna with triple-band elimination characteristics for super-wideband applications. *Sensors* **2020**, *20*, 624.

[27] Sharawi, M.S. Current misuses and future prospects for printed multiple-input, multiple-output antenna systems [Wireless Corner]. *IEEE Antennas Propag. Mag.* **2017**, *59*, 162–170.

[28] Gupta, K.C.; Garg, R.; Bahl, I.J. *Microstrip Lines and Solt Lines*. 2nd ed. Norwood, MA: Artech House, 1996.

[29] Mushiake, Y. A report on Japanese development of antennas: From the Yagi-Uda antenna to self-complementary antennas. *IEEE Antennas Propag. Mag.* **2004**, *46*, 47–60.

[30] Mushiake, Y. Self-complementary antennas. *IEEE Antennas Propag. Mag.* **1992**, *34*, 23–29.

[31] Rumsey, V. *Frequency Independent Antennas*. New York, NY, USA: Academic, 1966.

[32] Patre, S.R.; Singh, S.P. Broadband multiple-input–multiple-output antenna using castor leaf-shaped quasi-self-complementary elements. *IET Microw. Antennas Propag.* **2016**, *10*, 1673–1681.

[33] Blanch, S.; Romeu, J.; Corbella, I. Exact representation of antenna system diversity performance from input parameter description. *Electron. Lett.* **2003**, *39*, 705–707.

Pawan Kumar received the B.Tech. degree from Guru Gobind Singh Indraprastha University, New Delhi, India, and the M.Tech. degree from the Indian Institute of Technology Bombay, Mumbai, India, in 2012 and 2014, respectively. He was a recipient of the Post Graduate Fellowship from the Ministry of Education, India, and an Annual Scholarship from the Government of NCT of Delhi, India for his exemplary performance in the University Common Entrance Test. He received recognition from the Government of India for his contribution to Energy Technology Vision 2035, an initiative of the Technology and Information Forecasting Assessment Council (TIFAC), Department of Science and Technology (DST), India. His current research interests include the internet of things (IoT), machine learning, microwave sensing/imaging, and high-speed next-generation communication systems.

Shabana Urooj (Senior Member, IEEE) received the B.E. degree in electrical engineering and the M.Tech. degree in instrumentation and control from Aligarh Muslim University, Aligarh, India, in 1998 and 2003, respectively, and the Ph.D. degree in biomedical instrumentation from the Department of Electrical Engineering, Jamia Millia Islamia, New Delhi, India, in 2011. She has guided 07 Ph.D. and more than 68 M.Tech. dissertations. She has nearly three years of industry experience and over 18 years of teaching experience. She is currently working as an Associate Professor with the Department of Electrical Engineering, College of Engineering, Princess Nourah Bint Abdulrahman University, Riyadh, Saudi Arabia. She has authored and co-authored more than 120 research articles in high-quality international journals and conference proceedings. She is serving as a Member of the Standing Committee on Technical and Professional Development Activities. She was a recipient of the Springer's Excellence in Teaching and Research Award, the American Ceramic Society's Young Professional Award, the IEEE Region 10 Award for outstanding contribution in Educational Activities, Research Excellence Award from the Princess Nourah Bint Abdulrahman University in 2020, and several best paper

presentation awards. She is currently holding the responsibility of the Joint Secretary of the IEEE Delhi Section. She is holding the additional position of the Vice-Chair, Educational Activities of Saudi Arabia Section.

Areej Malibari (Member, IEEE) received the Ph.D. degree in computer science with a specialization in artificial intelligence and e-commerce from the University of Essex, United Kingdom, in 2010. She is the founder Dean of the College of Engineering, Princess Nourah Bint Abdulrahman University, Riyadh, Saudi Arabia. Dr. Areej served as an Honorary Lecturer in the School of Computer Science and Electronic Engineering, University of Essex, United Kingdom. She worked as the coordinator of ABET implementation, Vice Director of Computer Skills Unit, FCIT at King Abdulaziz University, Jeddah, Saudi Arabia. She has also served in administrative positions at the Saudi Electronic University-Female Campus, and the Strategic Office. She has published numerous research articles in high-quality and high impact factor journals and reputed international and national conferences. She has been instrumental in several International Leadership Management Certifications and Programs for Effective Motivational Leadership. She has received several international and national awards for her effective leadership and management. Her research interests include the internet of things (IoT), high-speed wireless communication, and artificial intelligence.